ADVANCES IN NUMERICAL MODELLING OF LINEAR FRICTION WELDED HIGH STRENGTH STEEL CHAINS

P. S. EFFERTZ*, F. FUCHS** and N. ENZINGER*

*Institute of Materials Science, Joining and Forming, Graz University of Technology, Kopernikusgasse 24/I, 8010 Graz, Austria
**pewag Austria GmbH, Mariazeller Straße 143, 8605 Kapfenberg, Austria

DOI 10.3217/978-3-85125-615-4-32

ABSTRACT

The linear friction welding process is an innovative solid state joining technology enabling high quality joints in chains, thus competing with the currently in use flash butt welding (FBW) process, with none of the drawbacks related to fusion welding processes. Modelling has proven to be an indispensable tool in LFW, providing necessary insight to the process due to its rapid nature. Furthermore, no need of expensive infrastructure, welding experimentsand subsequent testing is necessary. In this article, the current status of understanding and development in LFW of chains is presented via 2D and 3D models carried out in the commercial software DEFORM. The pre-processing steps are thoroughly described in terms of meshing characteristics, energy input analysis, boundary conditions, amongst others. As a result, various process outputs are presented, such as temperature evolution, flash morphology, material flow behaviour, and stress analysis. Experimental validation was carried out to assess the quality of the models. The models were able to predict the thermal evolution in the vicinity of the weld interface, as well as reproduce the phenomena behind flash formation and material flow. Finally, an outlook on numerical simulation of the process applied to chain welding is presented.

Keywords: Linear friction welding; chain welding, DEFORM; numerical simulation;

INTRODUCTION

Flash butt welding (FBW) is the process of preference regarding chain welding [1]. However, it is not without its drawbacks since FBW is a fusion process. Therefore, welding defects related to fusion joining processes such as, slug residues, porosity, segregation or hot cracking are prone to appear [1], [2]. To overcome the shortcomings related to FBW, linear friction welding has been a subject of research in chain welding over the recent years, since it provides very clean and reproducible welds, comprising exceptional mechanical properties [3].

Linear friction welding (LFW) is a solid-state joining process in which a stationary part is forced against another that is reciprocating in a linear manner to generate frictional heat [4], [5]. Heat, along with the axial compressive forces applied perpendicular to the weld

interface, results in material deformation and plasticization. Most of the plasticized material is removed from the weld through the flash, due to the combined action of applied force and reciprocating movement. Surface oxides and other asperities are expelled from the interface, producing a clean joint. This results in a loss of length of the overall component. Towards the end of the process the parts are forged together with some plasticized material remaining at the weld line [6].

Although the process is continuous, LFW can be split into four phases [7], [8].

In the **initial phase** the two surfaces are brought into contact under external load. Interaction between the surface asperities occurs, thus generating heat due to friction. The asperities soften and deform, increasing the true contact area between the two workpieces. In this phase, negligible axial shortening (burn-off) perpendicular to the oscillation direction is observed.

In the **transition phase** the material plasticizes and becomes viscous, causing the true contact area to increase until total surface contact is established. Heat from the interface is conducted to its vicinity, plasticizing more material, and burn-off starts to occur as a result of the expulsion of viscous material.

At this point, the force, thermal profile and burn-off reach a quasi-steady-state condition and significant burn-off occurs through the rapid expulsion of viscous material trough the interface. This phase is referred as the **equilibrium phase**.

Finally, during the deceleration phase the motion is ceased in a quick, however progressive manner, to ensure alignment between the workpieces. At that time the axial force is increased to forge the two components together, which give this phase its name: **forge phase**.

Computational modelling came a long way over the past few years, especially regarding Ti64 for aerospace applications, and more recently 30CrNiMo8 steel in the chain industry. It has proven to be an indispensable tool to give insight to the LFW process, which would not be possible with experiments alone [9], [10]. Various authors developed 2D [4], [9], [11]–[13] and 3D [14]–[18] computational models in order to predict various welding outputs, such as thermal fields [10], [13], [19], [20], flash morphology and formation rates [9], [14], [19], [21], residual stresses, strain rates [9] and microstructural characterization [22].

This paper aims to describe the numerical modelling advances within the scope of linear friction welded steel chains, by combining the advantages of 2D and 3D FEA efforts to evaluate and predict the intervening physical quantities of the process, such as temperature distribution, flash formation and shortening, and stress fields.

EXPERIMENTAL PROCEDURE

MATERIAL AND EQUIPMENT

The material used in the present study is a medium carbon 30CrNiMo8 high strength steel. The nominal chemical composition and mechanical properties at room temperature are given in table 1 and 2, respectively.

Dropforged half chain links were used with a cross-sectional width and height of 22 mm and 24 mm, respectively. Figure 1 illustrates the geometry of the used chain parts.

The main process parameters in LFW are the amplitude of oscillation, frequency of oscillation, and applied load during the friction and forging stages [23]. According to figure 1 the reciprocating movement is consistent with the x-direction, whereas the friction and forging load are applied along the y-direction.

Table 1 Chemical composition of 30CrNiMo8 (wt%) [24].

Elem.	C	Si	Mn	Cr	Mo	Ni	Fe
%	0.30	0.30	0.50	2.00	0.35	2.00	Bal.

Table 2 Mechanical properties of 30CrNiMo8 at room temperature.

E (GPa)	YS σ_y (MPa)	UTS (MPa)	ε (%)
210	1050	1250	9

The combination of parameters yielding the best mechanical properties was already optimized in previous investigations [3]. Hence, solely one combination is considered in the present study. Due to confidentiality reasons, the welding parameters are not presented.

The welds were carried out in a prototype machine, which is fully instrumented and allows the measurement of both normal and in-plane forces as well as displacements during the process.

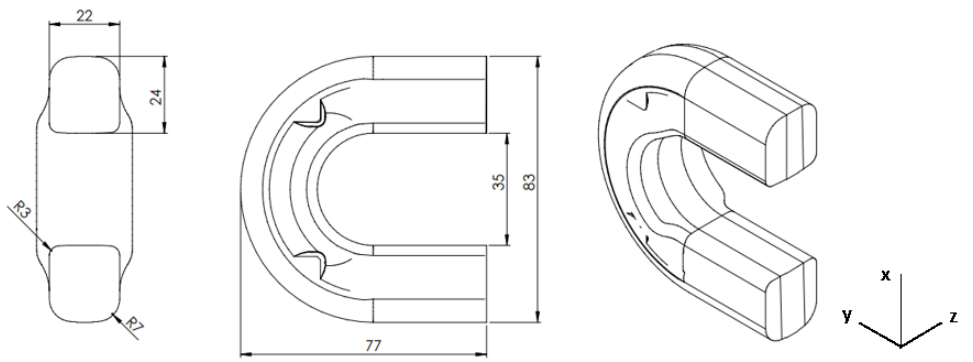

Fig. 1 Technical drawing of the used half chain link to be welded.

To characterize the weld and geometry of the flash, light optical microscope (LOM) was used to compare with the results yielded by the numerical model. The sample welded with the aforementioned best parameter combination was embedded in cold resin, ground using SiC paper from 120 grit to 4000, and polished with a diamond suspension 3 and 1 µm. Finally, the sample was etched using Nital 5%.

To validate the thermal evolution of the developed models, thermocouple measurements were carried out. To that end, three Ø0.3 mm K-type thermocouples were installed, equally

distanced from one another, placed at 3.6 mm, 4.0 mm and 4.8 mm from the interface. To fit the thermocouples, one of the links was cut in half and three Ø2.5 mm channels were milled perpendicular to the oscillation direction to accommodate the wiring. The thermocouple terminals were soldered at the desired position. Finally, the two halves were joined together and locally TIG welded as far away as possible from the weld interface, to avoid subjecting regions around the interface to thermal cycle and ensure their alignment throughout the process.

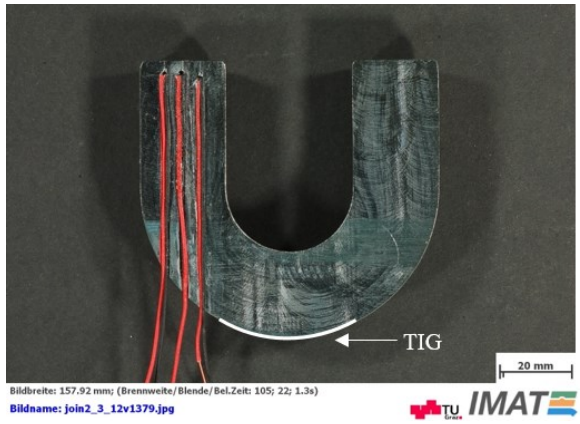

Fig. 2 Macrograph with the positioning of the thermocouples: 3.6 mm (left), 4.0 mm (centre) and 4.8 mm (right) from the interface. The tack welding position is indicated by the white line [25].

WELD ENERGY

Determining the energy given to the welding interface is of upmost importance to account for the friction component during the initial phase of the process. To that end, a similar approach to the one reported by Ofem et al. [26] is used, provided the fact that the machine is fully instrumented.

Using the recordings of in-plane load and displacement recorded by the machine, the energy input can be obtained. However, the load cell does not measure the in-plane load directly at the sample but rather between the clamping and servo-hydraulic system, as depicted schematically if figure 3. The instantaneous heat flux at the interface can be computed by,

$$\dot{q}'' = \frac{F_{\text{int}}^{net}(t)v(t)}{A(t)} \tag{1}$$

Where $F_{\text{int}}^{net}(t)$, $v(t)$ and $A(t)$ is the in-plane load, velocity at the interface and contact area between the half links, at a particular time step, respectively. Applying free body analysis to the system presented in figure 3, the load in the interface can be computed by,

$$F_{\text{int}}^{net} = F_{\text{int}}^{total} - Ma \tag{2}$$

Notwithstanding, the mass M of the oscillatory clamping system is unknown. Hence, the LFW machine was subjected to an unloaded run to account for the inertial movement and internal friction of the tooling system F_{int}^{0}. The load registered was then subtracted from the results obtained when the machine is loaded with a sample and equation 2 reduces to the following,

$$F_{\text{int}}^{net} = F_{\text{int}}^{total} - F_{\text{int}}^{0} \tag{3}$$

The preceding analysis requires an estimate of the velocity. This can be achieved numerically since the position at discrete values in time is known. Thus, the central finite difference is used for the first order derivative [27],

$$v(t) = \frac{\left| x_{t+\Delta t} - x_{t-\Delta t} \right|}{2\Delta t} \tag{4}$$

Where $x_{t+\Delta t}$ and $x_{t-\Delta t}$ denote the position at a previous and future time step; Δt stands for the time step size.

Finally, the total energy applied at the interface during a certain phase can be obtained as a result of the integration of equation over the phase duration t_{ph}.

$$E_{ph} = \int_{0}^{t_{ph}} \dot{q}'' A(t) dt \tag{5}$$

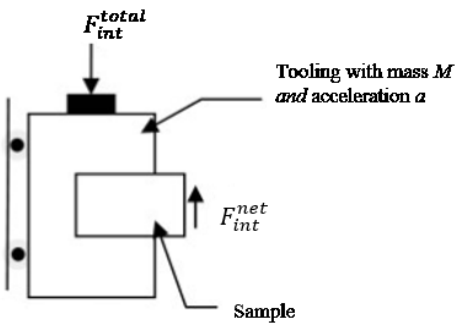

Fig. 3 Schematic diagram of the oscillating clamping system of an LFW machine [26].

MODELLING APPROACH

Numerical modelling of linear friction welded chains was conducted using finite element analysis (FEA) commercial software DEFORM-2D/3D 11.1 SP1. Similar to what is reported by McAndrew et al. [11], the "single-body" approach is used in both 2D and 3D models. Therefore, the numerical approach was divided into two models: purely thermal model and a coupled thermo-mechanical model. The first model represents the heating by friction in the initial phase of the process, thus serving as an initial thermal boundary condition for the thermo-mechanical model. This latter model accounts for the plastic deformation in the equilibrium phase. The mathematical formulation of the problem in hand is described in Annex A.

Unlike other studies, the initial phase during chain welding has considerable plastic deformation and is traduced in approximately 2 mm of burn-off, as reported in [25]. This has to do with the fact that the interfaces of the chains are not flat. However, deformation from the initial phase was not considered in this modelling approach. This assumption proved to be reliable, however it has to be considered during the evaluation. The models were ran until a burn-off of approximately 3 mm, which represent the total upset in the equilibrium phase.

MATERIAL MODEL

To describe the material behaviour in the 2D and 3D models, the tabular format provided by DEFORM software was used, due to its versatility and ability to represent any material. Temperature dependent thermal conductivity and heat capacity were obtained experimentally.

The material flow stress is given as a function of strain, strain-rate and temperature [28].

$$\bar{\sigma} = f\left(\bar{\varepsilon}, \dot{\bar{\varepsilon}}, T\right) \tag{6}$$

Stress-strain curves were obtained for temperatures, strains and strain-rates up to 1400°C, 4 and 1000 s-1, respectively. Gleeble 3800 was used to characterize material flow stresses at low strain-rates and JmatPro for estimating the values at high strain rates [29]. Logarithmic interpolation was considered whenever the models surpass the defined flow stress data.

MESH CHARACTERISTICS

In LFW most of the heat generation and plastic deformation throughout the process occurs along the weld interface. Thus for the 2D purely thermal model, an average element size of 0.2 mm was used within a 4 mm band around the interface. Outside this region, the element size was increased. The mesh of the thermo-mechanical model is obtained by merging and mirroring the purely thermal model along the interface. The mesh appearance is illustrated in figure 4(a)

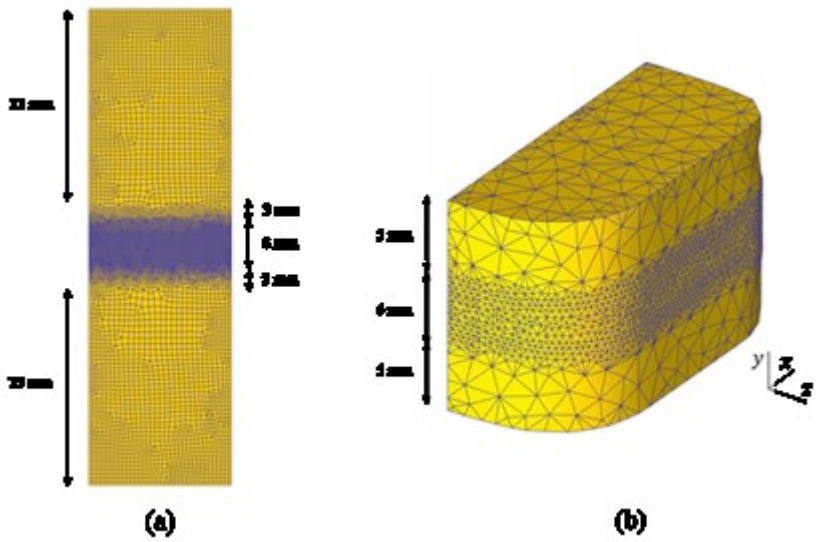

Fig. 4 Illustration of the mesh used for the thermo-mechanical models: (a) 2D model and (b) 3D model.

The 3D purely thermal and thermo-mechanical models were discretized using 4-node tetrahedral elements, which besides fitting better the geometry, are more stable for problems dealing with high deformations. Again, the mesh was refined in the areas of interest such as in the vicinity of the welding interface. Hence for the purely thermal model a width band with 3 mm close to the interface was considered, using elements with an average size of 0.5 mm. Similar element sizes were used by Gao et al. [17] and Pashazadesh et al. [30] when modelling friction stir spot and friction stir welding, respectively. The approach described in the 2D model was also carried out to the 3D one. Hence, the mesh used on the thermo-mechanical model is a result of mirror merging the purely thermal model at the interface, and is illustrated in figure 4 (b).

THERMAL MODELS

The thermal models account for the effect of frictional heat during the initial phase of the process. The developed 2D and 3D models are analogous, modelled with a single plastic workpiece, although differing slightly in the way heat input is applied at the interface.

In either models the heat flux is computed using equation presented in the section "Weld energy". As reported in [11], a uniform heat flux $\left(\dot{q}^{"}\right)$ was applied across most of the interface and only linearly reduced to 50% of this value from a distance away from the edge, corresponding to the amplitude. This reduction represents the effect of the oscillatory movement, where the offset between the workpieces means a lower heat input in the regions of the edges (see figure 5(a)).

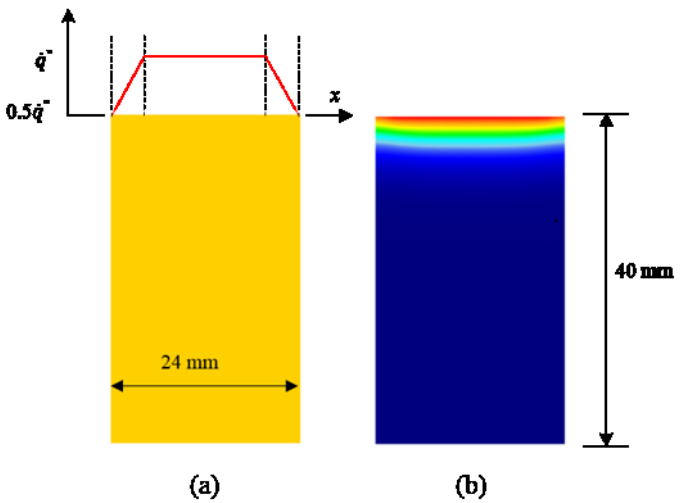

Fig. 5 2D thermal model: (a) applied heat flux profile; and (b) thermal profile generated at the end of the initial phase [25].

Regarding the 3D thermal model, the heat flux was not linearly reduced away from the edges, corresponding to the amplitude (a), as reported in the 2D model. Instead, a single step approach was used, where 50% of the value of $\left(\dot{q}^{"}\right)$ was used for half the amplitude near the edges. In order to maintain the mean energy due to contact/no-contact condition, 100% of $\left(\dot{q}^{"}\right)$ was considered for the remaining half of the amplitude value. Thus, the heat flux was applied as illustrated in Figure 6(a).

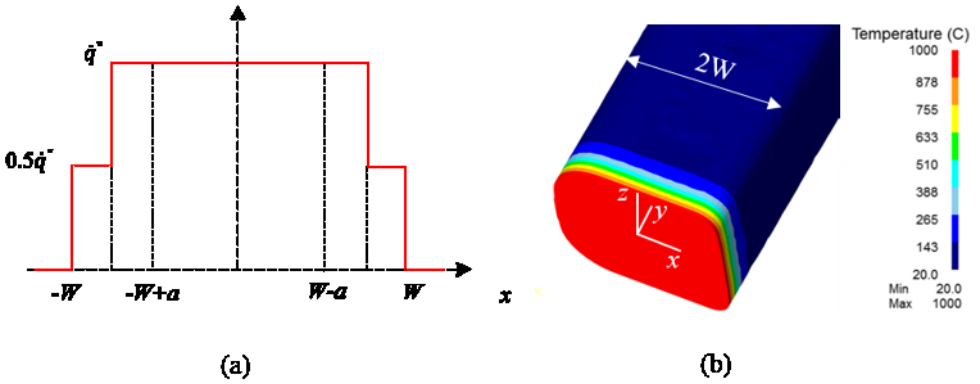

Fig. 6 3D thermal model: (a) applied heat flux profile; and (b) thermal profile generated at the end of the initial phase [31]

Emissivity was kept at default setting in both models, hence 0.7. The convective heat transfere between the workpiece and the surroundings assumed to be 20 W/(m^{2}K). Bulk and medium temperatures were set to 20 °C.

A simplification to the thermal model was made by not assuming the influence of the rounded edges in the overall interfacial contact throughout the process, hence the same heat flux profile was used in every point in the direction perpendicular to oscillating movement. The model was ran until a process time of 1.5s was reached, which corresponds to the end on the initial phase.

THERMO-MECHANICAL MODELS

The 2D thermo-mechanical was set up using a plastic workpiece and two rigid dies, illustrated in figure 7(a). Plain strain condition was assumed, as the dimension of the chain perpendicular to the oscillatory movement (22 mm) can be considered to be “much larger” that the material regions under viscoplastic condition (~3mm). Additionally, the amount of material being extruded in the direction perpendicular to the reciprocating movement is comparatively lower.. The model focuses on a small portion of the chain link, to reduce the number of elements employed and consequently computational time. The temperature profile obtained from the thermal model described in the previous section was mapped onto the plastic workpiece. The reciprocating movement and axial load is attributed to the upper and lower dies, respectively.

The 3D thermo-mechanical setup is analogous to 2D, apart from the fact that in the lower die the registered data of burn-off movement is used rather than load, as shown in figure 7(b). This approach enables the possibility to exploit the advantages of the Conjugate Gradient Solver, which, according to the DEFORM users’ manual, computationally more advantageous in terms of reduction of simulation time and storage.

Due to the symmetry of the process not only in relation to the interface but also the y direction, half of the deformable workpiece was used to reduce computational effort even further.

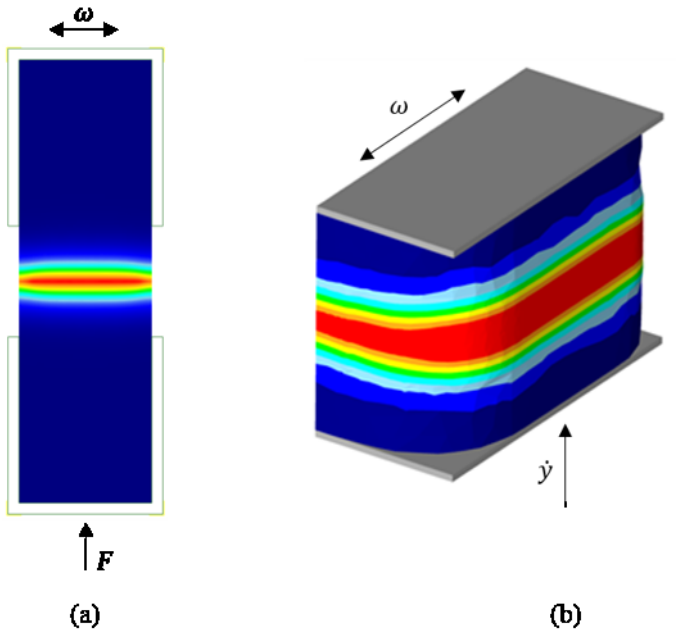

Fig. 7 Thermo-mechanical model showing a plastic single workpiece with a mapped thermal profile and applied boundary conditions: (a) 2D model; and (b) 3D model.

RESULTS AND DISCUSSION

THERMAL ANALYSIS

The thermal histories were recorded every 0.5 s at the corresponding upset position to assess the adequacy of the developed models, as presented in figure 8. The predicted temperatures are presented until the end of the equilibrium phase.

For the thermocouple closest to the interface, good agreement was obtained when compared to the predicted temperatures, as shown in figure 8(a). From t = 1 s to t = 2.5 s, the 3D model overestimated the temperature, and a maximum temperature difference of approximately 100°C registered at the beginning of the equilibrium phase (t =1.5 s).

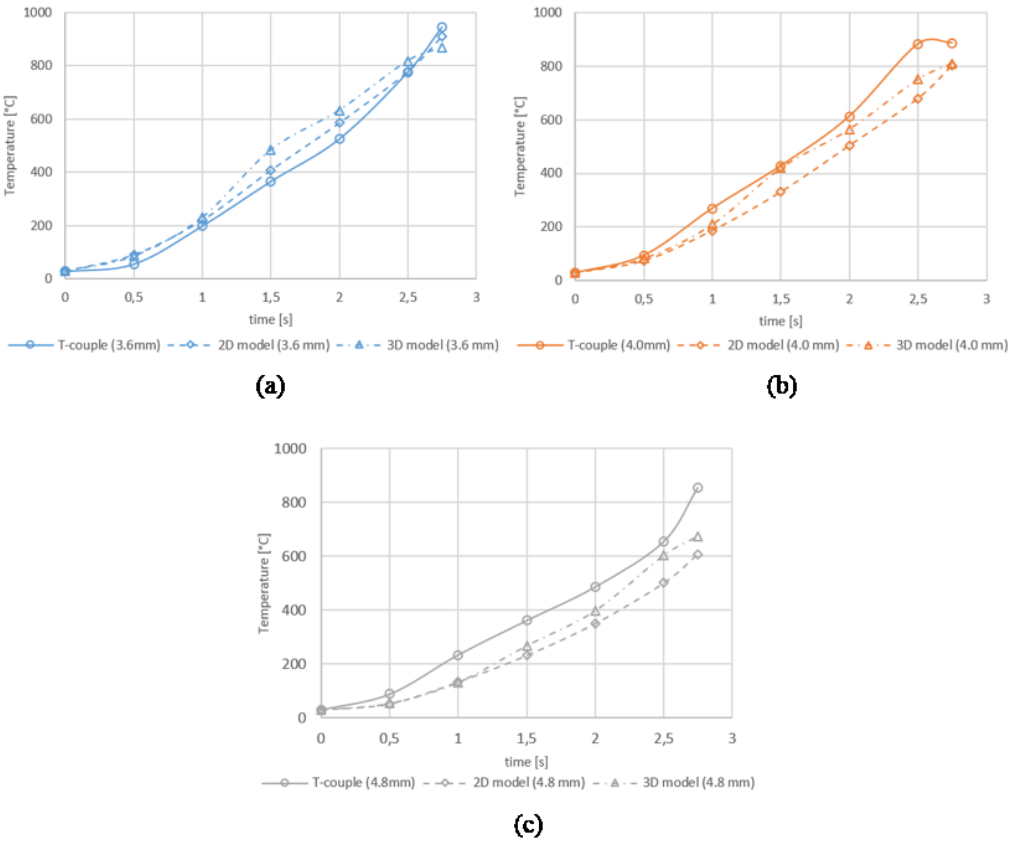

Fig. 8 Comparison of the thermal histories between experiment and models: (a) 3.6 mm; (b) 4.0 mm; and (c) 4.8 mm.

Adequate results were also obtained between the thermocouple initially at 4.0 mm and the models. Both models underestimated the temperature at $t = 2.5$ s. Worth mentioning is the fact that this particular thermocouple registered higher temperatures than the one closest to the interface. Although the thermocouples are mounted on the stationary part of the chain, they are under high cyclic stress due to the reciprocating movement and in-plane load. It is believed that the thermocouple did indeed move as a result, registering a higher temperature.

Finally, the highest discrepancy is acknowledged in the thermocouple furthest from the interface. However, the 3D model was able to predict more accurately the temperatures throughout the process, despite the differences at the end of the equilibrium phase.

FLASH FORMATION

The morphology and formation of the flash is directly related to the mechanisms driving the plastic deformation. Thus, the viscous material is expelled according to two main

mechanisms: (i) the axialload steadily extruding the viscous hot layer of material form between the workpieces; and (ii) the oscillatory motion dragging material from the weld line in each stroke of the oscillation. The prevailing effect is linked to the process parameters used, namely amplitude. Thus (i) is associated with low amplitudes, whereas (ii) with high amplitudes. Furthermore, larger oscillation amplitudes produces larger ripples in the flash. The rippling effect is a result of the interaction between viscoplastic material and vertical surface of the workpiece. The vertical surface therefore drags the viscoplastic material during the reciprocating movement, creating a distinct ripple [9].

In the present case the amplitude value is not high enough to shear the viscous material. Hence, mechanism (i) occurs and the extruded material remains in constant contact with the upper and lower workpiece during oscillation. Also, the thermal profile is wide enough to accommodate the difference in strain rates, and flow stresses associated, between the interface and material being sheared by the edge. As a result, a smooth flash without rippling is formed. Figure 9 depicts the comparison between the experimental and modelling results for the flash morphology.

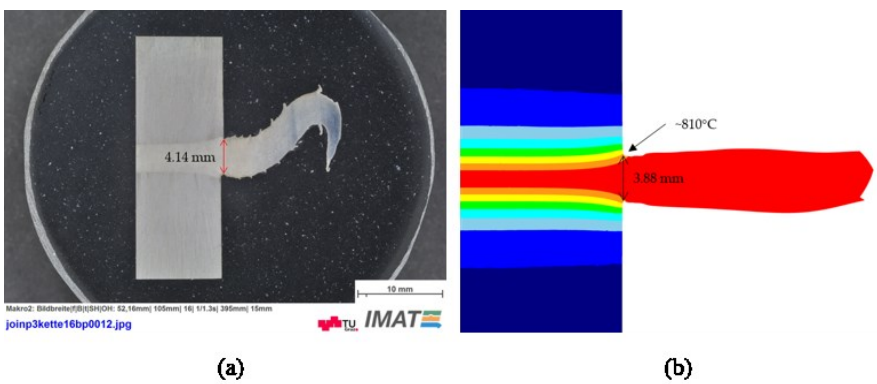

Fig. 9 Flash morphology comparison between the (a) experimental and (b) modelled flash.

The experimental flash in characterized by a smooth surface regardless of the small rippling which has not been reproduced by the model, since the element size used is not small enough to capture these features.

Moreover, the predicted flash shoes a rounded edge, in contrast with the sharp edge obtained in the experiment. This difference can be explained by the geometric properties of the chain links, as they are not completely flat as shown in figure 10. As a result, in the initial phase of the process this traduces in higher pressure and local heat input, consequently plasticizing locally the material in the interface.

The flash deflects upwards and downwards with the reciprocating movement, reaching its maximum height when the amplitude is at its maximum value. At a certain length, the flash contacts the tooling, causing it to bend as shown in figure 9(a). This behaviour was not observed in the model since there is no tooling interacting with the flash.

A relatively good agreement was obtained for the flash extrusion thickness, with 4.14 mm and 3.88 mm for the experiment and model, respectively. This difference might be due

to model related assumptions, such as meshing characteristics, heat input data; and material related, like flow stress and heat conductivity data.

Worthy of note, the model showed that the boundary temperature between flash formation and negligible material flow is approximately 810°C, as shown in figure 9(b). This temperature corresponds to the Ac3 temperature of this material.

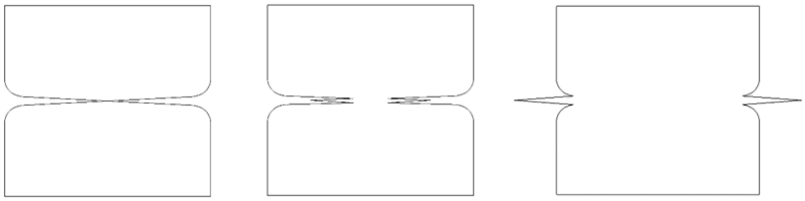

Fig. 10 Schematic representation of the evolution of the flash formation at the interface of the chain.

Analogous to the 2D flash formation, the extruded material remains in constant contact with the upper and lower parts of the workpiece during the oscillation movement, which characterizes welds with low amplitude, unable to promote shearing. The 3D model is invaluable to understand the multi directional material flow behaviour of the process, and figure 11 shows the morphology of the flash mirrored in the z-direction at different time steps.

Figure 11(a) shows the flash appearance in the early stages of the process. Also, until approximately t = 0.35 s, the flash distorts severely upwards and downwards with the oscillating movement. However, at a certain point despite the flipping movement of the flash, a preferential flow towards the moving part is acknowledged and is shown in figure 11(b). This tendency might be related due to the constant constraints imposed on the flash by self-contact and tooling contact, promoting local shearing on the base of the flash, which coupled with the pressure increase at high amplitudes redirects the flash to the moving side. Furthermore, the deflection of the flash might also be a product of the tooling effect entitled “micro-swinging”. Hence, the moving part of the chain does not move rigidly in the oscillation direction, but has a micro-swing relative to the oscillation plane instead. According to Li et al. [32] micro-swinging has a significant effect of the extrusion manner, as the swinging part ends up digging into the other promoting deflection of the flash from its centre point. On the other hand, negligible effect on the interface temperature at the centre of the weld. This phenomena can also observed in the experimental flash, according to the figure 9(a). Notice that the flash near to the extrusion zone also diverts upwards.

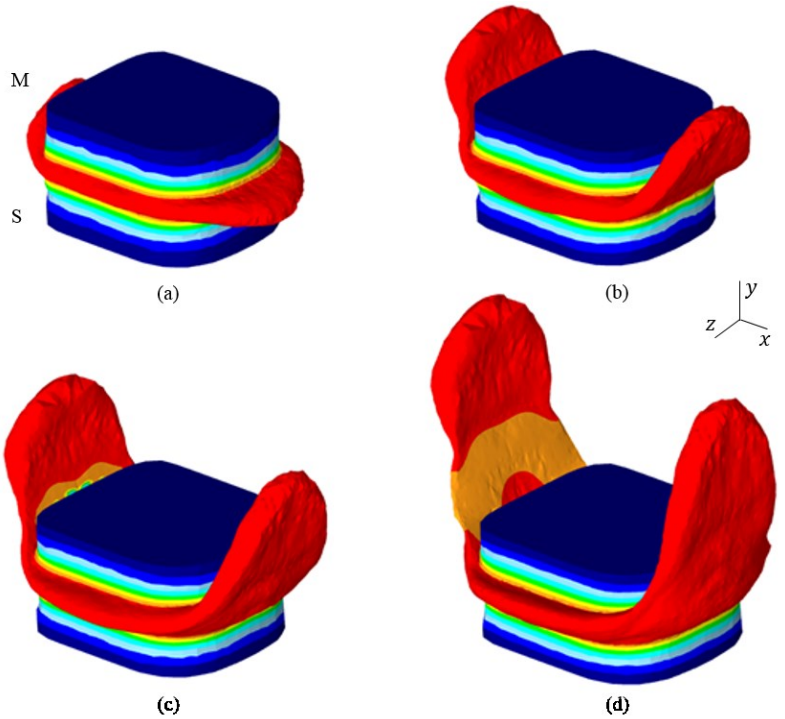

Fig. 11 Appearance of the formed flash through different time steps: (a) t = 0.25 s; (b) t = 0.50 s; (c) t = 0.75 s; and (d) t = 0.90 s. 'S' and 'M' denote the stationary and moving components, respectively.

A further consequence of the flash extrusion evolution has to do with the self-contact observed at a certain point of the simulation process as the flash contacts the workpiece. As a result, conduction heat transfer occurs locally, causing the uneven cooling of the flash as shown in figure 11(c). Moreover, by the end of the equilibrium phase t = 0.90 s illustrated in figure 11(d), one can intuitively acknowledge that the flash further away from the extrusion zone is locally colder when compared to other regions due to convection and the influence of conduction from earlier stages.

Partial unbonding

The partial unbonding phenomena was observed in the developed 3D model at low burn-off values, as depicted in figure 12. This particularity was also reported by McAndrew et al. [33] and Addison [34], and is known to compromise mechanical properties, ultimately leaving a notch that acts as a crack propagation site. Unbonding was observed solely in the corners of the cross-section with lower radii, suggesting that there might be a critical radius at which partial unbonding is prone to occur. Nonetheless, as the model progressed the heat provided to these regions provided by the flash and interface due to conduction, caused the corners to soften and plastically deform, thus resulting in a defect free bond.

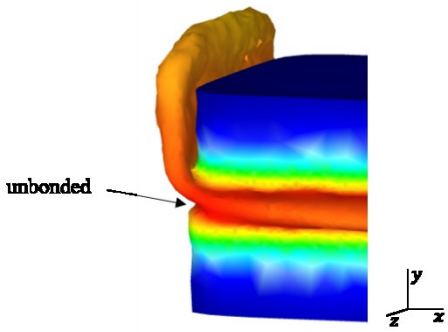

Fig. 12 FEA appearance of partial unbonding at the interface [31].

BURN-OFF ANALYSIS

The interest in studying and predicting the rate of material expelled as flash is of great importance, as it is related to the upsetting process. To that end, a burn-off analysis was solely carried out to the 2D model since it is load controlled, whereas the 3D model is stroke controlled. Hence, in the latter case makes no sense to study the burn-off rate.

To evaluate the burn-off throughout the process, point tracking was used, as shown in figure 13 specified by P_1. The model predicted a linear axial shortening, typical of the LFW process in the equilibrium phase, where quasi-steady state conditions are achieved in steel. Figure 14 relates the burn-off as a function of time for the experiment and model. A comparable result is acknowledged, with an experimental and predicted burn-off rate of 3.08 mm/s and 3.13 mm/s, respectively. Despite the good agreement, it is clear that in the initial instants of the equilibrium phase the model does not upset in the same rate as experimentally, which suggests that the prescribed interface temperature resulting from the purely thermal model is low. Hence, the material flow until 0.25 s was underestimated. Steady state burn-off is observed throughout the remainder of the equilibrium phase and comparable upset was reached between model and experiment.

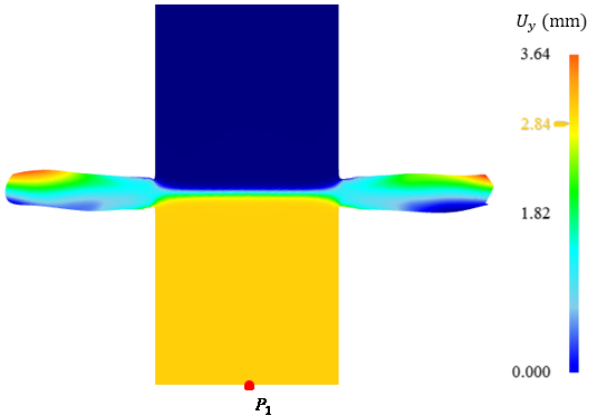

Fig. 13 2D FEA axial displacement with point tracking P_1.

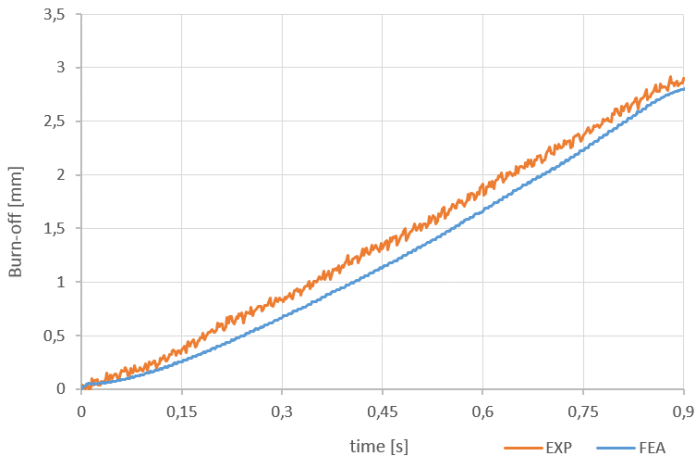

Fig. 14 Comparison between experimental and predicted burn-off histories.

CONCLUSIONS

A summary of the main findings and advances in LFW of chains, followed by an outlook for further research within this subject, is presented in this section. This should allow the reader to appreciate the benefits of numerical modelling in LFW process for joining 30CrNiMo8 high strength steel chains, envisioning further process development and exploitation.

SUMMARY

This paper describes the use of 2D and 3D modelling approaches to evaluate and predict the intervening physical quantities of the LFW process when joining 30CrNiMo8 high strength steel half chain links. The key findings and advances are listed below:

- Comparable results were obtained with thermocouple measurements and FE models. Nonetheless, a slight temperature offset was acknowledged for the setting furthest from the interface. In all situations, the temperature predicted by the 3D model is slightly higher than the 2D model.
- A 2D and 3D finite element modelling for the LFW of 30CrNiMo8 high strength steel chains has been formulated, using an optimized welding parameter combination, in order to predict the thermal and mechanical characteristics. This was achieved by means of a purely thermal and thermo-mechanical model. A very good agreement between reality and model was achieved without application of a single fit parameter.
- For either models, the flash showed a smooth morphology which is in accordance with experimental observation apart from the slight rippling effect observed in the experiment. This smooth pattern in the simulation is related to low process parameters which yield low energy input.
- The local plasticization of the material due to the uneven surface of the experimental interface meant that the morphology of edges between experimental and predicted flash did not match perfectly.
- The mechanism that prevails for the set of parameters in this study, is dictated by the forging load, steadily extruding viscous material from the interface.
- Partial unbonding phenomena was observed via the 3D model, solely in the corners of the cross-section with lower radii, suggesting that there might be a critical radius at which partial unbonding can occur. However, unbonding proved not to be an issue as the process heat input is high enough. Partial unbonding was only observed for low burn-off values.
- The 2D model predicted a linear axial shortening, typical of the LFW process in the equilibrium phase, where quasi-steady state conditions are achieved. Very good agreement was obtained with an experimental and predicted burn-off rate of 3.08 mm/s and 3.13 mm/s, respectively.

OUTLOOK

Despite the recent advances in modelling and comprehending the linear friction welding process applied to chains, there are still several knowledge gaps that need to be tackled. Some of which are:

- Residual stress analysis: modelling can be used to predict the impact of the processing conditions, such as the workpiece geometry, amplitude, frequency, axial load, on the formation and magnitude of residual stresses in linear friction welds. Figure shows some preliminary results on residual stresses after cooling and before PWHT. However, the next step is to validate the obtained results.

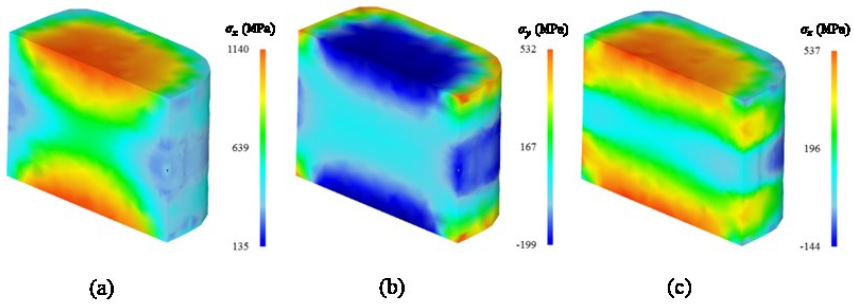

Fig. 15 FEA results for residual stresses: (a) σ_x ; (b) σ_y ; and (c) σ_z .

- Microstructure modelling: Models could be used to investigate the impact of the processing conditions on the microstructure evolution. This would allow for the effects of the processing conditions on different phases, average grain size and their spatial distribution [35].
- Influence of interface geometry: Most of the modelling effort has been put into planar interface geometries. However, the influence of the interface geometry (e.g. bevels angles) on LFW chains should be assessed and optimized to reduce flash formation and ultimately curtail the amount of scrap generated during production.

ACKNOWLEDGEMENTS

The authors gratefully acknowledge the financial support of this work by the project JOIN. The K-Project Network of Excellence for Joining Technologies JOIN is fostered in the frame of COMET – Competence Centers for Excellent Technologies by BMVIT, BMWFJ, FFG, Land Oberöstereich, Land Steiermark, SFG and ZIT. The program COMET is handled by FFG.

ANNEX A. MATHEMATICAL FORMULATION

The thermal analysis is governed by the diffusion equation with thermo-mechanical heat source term given by equation [36].

$$\rho c_p \dot{T} = \left(kT_{,i}\right)_{,i} + \eta \sigma_{ij} \dot{\varepsilon}_{ij} \tag{7}$$

Where c_p is the specific heat capacity, k the thermal conductivity, σ_{ij} the stress tensor and $\dot{\varepsilon}_{ij}$ is the strain rate tensor. The terms $\rho c_p \dot{T}$ and $\left(kT_{,i}\right)_{,i}$ represent the internal energy and heat transfer rates, respectively. "$,i$" denotes the differentiation in i. The energy balance can be rewritten in the variational form as [37]:

$$\int_V kT_{,i}\delta T_{,i} + \int_V \rho c_p \dot{T} dV - \int_S q_n \delta T dS - \int_V \eta \sigma_{ij} \dot{\varepsilon}_{ij} \delta T dS = 0 \tag{8}$$

where q_n is the heat flux over surface S. The term η is related to the fraction of mechanical work that is converted into heat, which in the case of the purely thermal model is not considered, as no plastic deformation is considered. In this case equation 7 reduces to:

$$\int_V kT_{,i}\delta T_{,i} + \int_V \rho c_p \dot{T} dV - \int_S q_n \delta T dS \tag{9}$$

It is, however, taken into account in the thermo-mechanical model and assumed to be η =0.9. The fraction of remainder plastic deformation energy is associated with changes in dislocation density, (sub-)grain boundary generation and migration, and phase transformation and evolution [30].
In an FE framework, the energy balance can be discretized into:

$$[C]\{\dot{T}\} + [K]\{T\} = \{Q\} \tag{10}$$

where $[C]$ is the heat capacity matrix, $[K]$ the conductivity matrix, $\{Q\}$ the vector accounting for all thermal sources in the system, $\{T\}$ and $\{\dot{T}\}$ are the nodal temperature and temperature rate vectors, respectively.
The temperature rate at the beginning of a time increment can be obtained according to equation 10.

$$\{\dot{T}\}_i = [C]^{-1}(\{Q\} - [K]\{T\}_i) \tag{11}$$

DEFORM uses an implicit dynamic procedure designed form metal forming processes. Thus, the temperature equation can be given as [38], [39]:

$$\{T\}_{i+1} = \{T\}_i + \Delta t\left((1-\beta)\{\dot{T}\}_i + \beta\{\dot{T}\}_{i+1}\right) \tag{12}$$

Where β specifies the forward integration coefficient for temperature integration over time, and varies between 0 and 1. The default value of 0.75 is adequate for most simulations [28].

Regarding the mechanical analysis, rigid-viscoplastic finite element approach was considered using the variational principle.

The rigid-viscoplastic material is an idealization of an actual one, by neglecting the elastic response. The rigid viscoplastic material, which was introduced for the analytical convenience, simplifies the solution process with less demanding computational procedure. Moreover, it seems that the idealization offers excellent solution accuracies due to the negligible effects of elastic response at large strain in the actual material. Hence, this

simplification is especially suitable for metal forming analysis at high temperatures, in which LFW is included [40].

The variational approach requires that among admissible velocities u_i that satisfy the conditions of compatibility and incompressibility, as well as velocity boundary conditions, the actual solution gives the following functional a stationary value [41]:

$$\pi = \int_V E\left(\dot{\varepsilon}_{ij}\right)dV - \int_{S_F} F_i u_i dS \tag{13}$$

where F_i represents surface tractions, and $E\left(\dot{\varepsilon}_{ij}\right)$ is the work function expressed by [42]:

$$E\left(\dot{\varepsilon}\right) = \int_0^{\dot{\bar{\varepsilon}}} \bar{\sigma} d\dot{\bar{\varepsilon}} \tag{14}$$

where $\bar{\sigma}$ is the effective stress, and $\dot{\bar{\varepsilon}}$ is the effective strain-rate. The solution of the original boundary-value problem is then obtained from the solution of the dual variational problem, where the first-order variation of the functional vanishes, namely,

$$\delta\pi = \int_V \bar{\sigma}\delta\dot{\bar{\varepsilon}} dV - \int_{S_F} F_i \delta u_i dS = 0 \tag{15}$$

with $\bar{\sigma} = \bar{\sigma}\left(\bar{\varepsilon}, \dot{\bar{\varepsilon}}\right)$ for rigid-viscoplastic materials. The incompressibility constraint on admissible velocity fields is removed by introducing a penalized form of the incompressibility in the variation of the functional. Therefore, the actual velocity field is determined from the stationary value of the variation as follows [15],

$$\delta\pi = \int_V \bar{\sigma}\delta\dot{\bar{\varepsilon}} dV + K\int_V \dot{\varepsilon}_\upsilon \delta\dot{\varepsilon}_\upsilon - \int_{S_F} F_i \delta u_i dS = 0 \tag{16}$$

where K is the penalty constant, which should be a large positive value for incompressibility; and $\dot{\varepsilon}_\upsilon = \dot{\varepsilon}_{ii}$ is the volumetric strain-rate [41].

REFERENCES

[1] K. MUCIC, N. ENZINGER, AND F. FUCHS, "Linear Friction Welding of High Strength Chains," *Trends Weld. Res. Proc. 9th Int. Conf.*, pp. 752–756, 2013.

[2] C. ÇETINKAYA AND U. ARABACI, "Flash butt welding application on 16MnCr5 chain steel and investigations of mechanical properties," *Mater. Des.*, vol. 27, no. 10, pp. 1187–1195, 2006.

[3] K. MUCIC, F. FUCHS, AND N. ENZINGER, "Process optimization for linear friction welding of high strength chain," in *EUROJOIN Conference*, 2012, pp. 157–166.

[4] X. Song, M. Xie, F. Hofmann, T. S. Jun, T. Connolley, C. Reinhard, R. C. Atwood, L. Connor, M. Drakopoulos, S. Harding, and A. M. Korsunsky, "Residual stresses in Linear Friction Welding of aluminium alloys," *Mater. Des.*, vol. 50, pp. 360–369, 2013.

[5] I. Bhamji, M. Preuss, P. L. L. Threadgill, and A. C. C. Addison, "Solid state joining of metals by linear friction welding: a literature review," *Mater. Sci. Technol.*, vol. 27, no. 1, pp. 2–12, 2011.

[6] I. Bhamji, M. Preuss, R. J. Moat, P. L. Threadgill, and A. C. Addison, "Linear friction welding of aluminium to magnesium," *Sci. Technol. Weld. Join.*, vol. 17, no. 5, pp. 368–374, 2012.

[7] A. Vairis and M. Frost, "On the extrusion stage of linear friction welding of Ti 6Al 4V," *Mater. Sci. Eng. A*, vol. 271, no. 1–2, pp. 477–484, 1999.

[8] A. Vairis and M. Frost, "High frequency linear friction welding of a titanium alloy," *Wear*, vol. 217, no. 1, pp. 117–131, 1998.

[9] R. Turner, J. C. Gebelin, R. M. Ward, and R. C. Reed, "Linear friction welding of Ti-6Al-4V: Modelling and validation," *Acta Mater.*, vol. 59, no. 10, pp. 3792–3803, 2011.

[10] A. R. McAndrew, P. A. Colegrove, A. C. Addison, B. C. D. Flipo, and M. J. Russell, "Energy and Force Analysis of Ti-6Al-4V Linear Friction Welds for Computational Modeling Input and Validation Data," *Metall. Mater. Trans. A Phys. Metall. Mater. Sci.*, vol. 45, no. 13, pp. 6118–6128, 2014.

[11] A. R. McAndrew, P. A. Colegrove, A. C. Addison, B. C. D. Flipo, and M. J. Russell, "Modelling the influence of the process inputs on the removal of surface contaminants from Ti-6Al-4V linear friction welds," *Mater. Des.*, vol. 66, no. PA, pp. 183–195, 2015.

[12] A. Vairis and M. Frost, "Modelling the linear friction welding of titanium blocks," *Mater. Sci. Eng. A*, vol. 292, no. 1, pp. 8–17, 2000.

[13] W.-Y. Li, T. Ma, and J. Li, "Numerical simulation of linear friction welding of titanium alloy: Effects of processing parameters," *Mater. Des.*, vol. 31, no. 3, pp. 1497–1507, 2010.

[14] J. Sorina-Müller, M. Rettenmayr, D. Schneefeld, O. Roder, and W. Fried, "FEM simulation of the linear friction welding of titanium alloys," *Comput. Mater. Sci.*, vol. 48, no. 4, pp. 749–758, 2010.

[15] G. Buffa, M. Cammalleri, D. Campanella, and L. Fratini, "Shear coefficient determination in linear friction welding of aluminum alloys," *Mater. Des.*, vol. 82, pp. 238–246, 2015.

[16] Y. Mao, L. Ke, F. Liu, Q. Liu, C. Huang, and L. Xing, "Effect of tool pin eccentricity on microstructure and mechanical properties in friction stir welded 7075 aluminum alloy thick plate," *Mater. Des.*, vol. 62, pp. 334–343, 2014.

[17] Z. Gao, J. T. Niu, F. Krumphals, N. Enzinger, S. Mitsche, and C. Sommitsch, "FE modelling of microstructure evolution during friction stir spot welding in AA6082-T6," *Weld. World*, vol. 57, no. 6, pp. 895–902, 2013.

[18] W. Li, F. Wang, S. Shi, T. Ma, J. Li, and A. Vairis, "3D Finite Element Analysis of the Effect of Process Parameters on Linear Friction Welding of Mild Steel," *J. Mater. Eng. Perform.*, vol. 23, no. 11, pp. 4010–4018, 2014.

[19] E. Ceretti, L. Fratini, C. Giardini, and D. La Spisa, "Numerical modelling of the linear friction welding process," *Int. J. Mater. Form.*, vol. 3, no. SUPPL. 1, pp. 1015–1018, 2010.

[20] R. Turner, R. M. Ward, R. March, and R. C. Reed, "The magnitude and origin of residual stress in Ti-6Al-4V linear friction welds: An investigation by validated numerical modeling," *Metall. Mater. Trans. B Process Metall. Mater. Process. Sci.*, vol.

43, no. 1, pp. 186–197, 2012.
[21] F. SCHROEDER, R. M. WARD, R. P. TURNER, M. M. ATTALLAH, J. GEBELIN, AND R. C. REED, "Linear friction welding of titanium alloys for aeroengine applications: modelling and validation," *9th Int. Conf. Trends Weld. Res.*, no. January, pp. 886 – 892, 2012.
[22] M. GRUJICIC, R. YAVARI, J. S. SNIPES, S. RAMASWAMI, C. F. YEN, AND B. A. CHEESEMAN, "Linear friction welding process model for carpenter custom 465 precipitation-hardened martensitic stainless steel," *J. Mater. Eng. Perform.*, vol. 23, no. 6, pp. 2182–2198, 2014.
[23] M. MAALEKIAN, "Friction welding - critical assessment of literature," *Sci. Technol. Weld. Join.*, vol. 12, no. 8, pp. 738–759, 2007.
[24] BÖHLER, "Heat Treatable Steel Böhler V145."
[25] P. S. EFFERTZ, F. FUCHS, AND N. ENZINGER, "Modelling the flash formation of linear friction welded 30CrNiMo8 high strength steel chains," *Int. J. Adv. Manuf. Technol.*, 2017.
[26] U. U. OFEM, P. A. COLEGROVE, A. ADDISON, AND M. J. RUSSELL, "Energy and force analysis of linear friction welds in medium carbon steel," *Sci. Technol. Weld. Join.*, vol. 15, no. 6, pp. 479–485, 2010.
[27] E. KREYSZIG, *Advanced Engineering Mathematics: Maple Computer Guide*, 8th ed. New York, NY, USA: John Wiley & Sons, Inc., 2000.
[28] SFTC, "DEFORM v11.1 SP1 System Documentation." .
[29] M. STUMMER, "Eigenschaften von 30CrNiMo8 für die Simulation," TU Graz, 2014.
[30] H. PASHAZADEH, J. TEIMOURNEZHAD, AND A MASOUMI, "Numerical investigation on the mechanical, thermal, metallurgical and material flow characteristics in friction stir welding of copper sheets with experimental verification," *Mater. Des.*, vol. 55, no. March, pp. 619–632, 2014.
[31] P. EFFERTZ, F. FUCHS, AND N. ENZINGER, "3D Modelling of Flash Formation in Linear Friction Welded 30CrNiMo8 Steel Chain," *Metals (Basel).*, vol. 7, no. 10, p. 449, 2017.
[32] W. LI, J. GUO, X. YANG, T. MA, AND A. VAIRIS, "The effect of micro-swinging on joint formation in linear friction welding," *J. Eng. Sci. Technol. Rev.*, vol. 7, no. 5, pp. 55–58, 2014.
[33] A. R. MCANDREW, P. A. COLEGROVE, B. C. D. FLIPO, AND C. BÜHR, "3D modelling of Ti-6Al-4V linear friction welds," *Sci. Technol. Weld. Join.*, no. December, pp. 1–9, 2016.
[34] A. C. ADDISON, "Linear friction welding information for production engineering," *TWI Industrial Member Report Summary*, vol. 961, TWI, Granta Park, UK, 2010.
[35] A. R. MCANDREW, P. A. COLEGROVE, C. BÜHR, B. C. D. FLIPO, AND A. VAIRIS, "A literature review of Ti-6Al-4V linear friction welding," *Prog. Mater. Sci.*, vol. 92, no. October, pp. 225–257, 2018.
[36] H. SCHMIDT AND J. HATTEL, "A local model for the thermomechanical conditions in friction stir welding," *Model. Simul. Mater. Sci. Eng.*, vol. 13, no. 1, pp. 77–93, 2005.
[37] L. YANG, "Modelling of the Inertia Welding of Inconel 718," *Dep. Metall. Mater.*, no. January, p. 160, 2010.
[38] J. S. SUN, K. H. LEE, AND H. P. LEE, "Comparison of implicit and explicit finite element methods for dynamic problems," *J. Mater. Process. Technol.*, vol. 105, no. 1–2, pp. 110–118, 2000.
[39] T. J. R. HUGHES, *The Finite Element Method: Linear Static and Dynamic Finite Element Analysis (Dover Civil and Mechanical Engineering)*. Dover Publications, 2000.
[40] S. I. OH, "Finite element analysis of met al forming processes with arbitra rily shaped dies," *Int. J. Mech. Sci.*, vol. 24, no. 8, pp. 479–493, 1982.
[41] S. KOBAYASHI, S.-I. OH, AND T. ALTAN, "Metal forming and the finite element method ,"

vol. 4 . Oxford Univ. Press , New York, NY [u.a.] , 1989.

[42] R. HILL, “New horizons in the mechanics of solids,” *J. Mech. Phys. Solids*, vol. 5, pp. 66–74, 1956.